

Gravitational collapse of a magnetized fermion gas with finite temperature

I. Delgado Gaspar¹, A. Pérez Martínez², Roberto A. Sussman³, and A. Ulacia Rey^{3,4}

¹ Instituto de Geofísica y Astronomía (IGA), Calle 212 No 2906, La Lisa, La Habana, 11600, Cuba, e-mail: idelgado@iga.cu

² Instituto de Cibernética, Matemática y Física (ICIMAF), Calle E esq 15 No. 309 Vedado, La Habana, 10400, Cuba, e-mail: aurora@icmf.inf.cu

³ Instituto de Ciencias Nucleares, Universidad Nacional Autónoma de México (ICN-UNAM). A. P. 70–543, 04510 México D. F., e-mail: sussman@nucleares.unam.mx

⁴ Instituto de Cibernética, Matemática y Física (ICIMAF), Calle E esq 15 No. 309 Vedado, La Habana, 10400, Cuba, e-mail: alain@icmf.inf.cu

Received: date / Revised version: date

Abstract. We examine the dynamics of a self-gravitating magnetized electron gas at finite temperature near the collapsing singularity of a Bianchi-I spacetime. Considering a general and appropriate and physically motivated initial conditions, we transform Einstein–Maxwell field equations into a complete and self-consistent dynamical system amenable for numerical work. The resulting numerical solutions reveal the gas collapsing into both, isotropic (“point-like”) and anisotropic (“cigar-like”) singularities, depending on the initial intensity of the magnetic field. We provide a thorough study of the near collapse behavior and interplay of all relevant state and kinematic variables: temperature, expansion scalar, shear scalar, magnetic field, magnetization and energy density. A significant qualitative difference in the behavior of the gas emerges in the temperature range $T \sim 10^4\text{K}$ and $T \sim 10^7\text{K}$.

PACS. 0 4.20.-q, 04.40.+b, 05.30.Fk

1 Introduction

Astrophysical systems provide an ideal scenario to examine the effects of strong magnetic fields associated with self-gravitating sources under critical conditions. In such conditions, we expect non-trivial coupling between gravitation and other fundamental interactions (strong, weak and electromagnetic), and from this interplay important clues of their unification could emerge.

The presence and effects of strong magnetic fields in compact objects (neutron, hybrids and quark stars) have been studied in the literature (see [1,2,3,4,5,6,7,8], and references quoted therein), assuming various types of equations of state (EOS) has been obtained and considering in some of these papers numerical solutions of the equilibrium Tolman–Oppenheimer–Volkov (TOV) equation.

As proven in previous work [1,8,9,10,11], the presence of a magnetic field is incompatible with spherical symmetry and necessarily introduces anisotropic pressures. However, by assuming that anisotropies and deviations from spherical symmetry remain small, several authors [8,10,12] have managed to compute observable quantities of idealized static and spherical compact objects under the presence of strong magnetic fields by means of TOV equations that incorporate these anisotropic pressures. Moreover, it is evident that much less idealized models would result

by considering the magnetic field and its associated pressure anisotropies in the context of TOV equations under axial symmetric (or at least cylindrically symmetric) geometries [8].

As an alternative (though still idealized) approach, and bearing in mind the relation between magnetic fields and pressure anisotropy, we have examined the dynamics of magnetized self-gravitating Fermi gases as sources of a Bianchi I space-time [13,14,15], as this is the simplest non-stationary geometry that is fully compatible with the anisotropy produced by magnetic field source.

Evidently, a Bianchi I model is a completely inadequate metric for any sort of a compact object, as all geometric and physical variables depend only on time (and thus it cannot incorporate any coupling of gravity with spatial gradients of these variables). However, the use of this idealized geometry could still be useful to examine qualitative features of the local behavior of the magnetized gas under special and approximated conditions. Specifically, we aim at providing qualitative results that could yield a better understanding of the conditions approximately prevailing near the center and the rotation axis of less idealized configurations, where the angular momentum of the vorticity and the spatial gradients of the 4-acceleration and other key variables play a minor dynamical role.

The main objective of the present paper is to study the dynamical evolution of a self-gravitating magnetized Fermi gas at finite temperature, under the extremely critical conditions near a collapsing singularity. In particular, we examine the possibility that a finite temperature may produce the dynamical effect of “slowing down” or reversing the collapse of the magnetized gas. Also, we aim at verifying how a finite temperature affects the evolution of other thermodynamic variables, such as the magnetization and energy density. This work constitutes a continuation and enhancement of previous work [13].

The paper is organized as follow. In section II we derive the EOS for a dense magnetized electron gas at finite temperature. In section III we lay out the dynamical equations for the evolution of our model by writing up the Einstein–Maxwell system of equation for the specific source under consideration. In section IV we introduce the local kinematic variables, which are later used in section V to write the Einstein–Maxwell equations as a system of non-linear autonomous differential equations, rewriting it afterwards in terms of physically motivated dimensionless variables. The numerical analysis of the collapsing solutions and the discussion of the physical results are given in the section VI. Our conclusions are presented in sections VII.

2 Magnetized Fermi gas as a source of a Bianchi I background geometry

Homogeneous but anisotropic Bianchi I models are described by the Kasner metric¹

$$ds^2 = -dt^2 + Q_1(t)^2 dx^2 + Q_2(t)^2 dy^2 + Q_3(t)^2 dz^2, \quad (1)$$

so that spatial curvature vanishes and all quantities depend only on time. Assuming a comoving frame with coordinates $x^a = [t, x, y, z]$ and 4-velocity $u^a = \delta_t^a$, the energy–momentum tensor for a self-gravitating magnetized gas of free electrons is given by:

$$T_b^a = (U + P) u^a u_b + P \delta_b^a + \Pi_b^a, \quad P = p - \frac{2BM}{3}, \quad (2)$$

where B is the magnetic field (pointing in the z direction), U is the energy density (including the rest energy of the electrons), $M = -(\partial\Omega/\partial B)$ with $\Omega = \Omega_e + B^2/2$ and Ω_e is the thermodynamical potential of the electron gas, P is the isotropic pressure and Π_b^a is the traceless anisotropic pressure tensor:

$$\Pi_b^a = \text{diag}[0, \Pi, \Pi, -2\Pi], \quad \Pi = -\frac{BM}{3}, \quad (3)$$

We can write the energy–momentum (2) tensor as:

$$T_b^a = \text{diag}[-U, P_\perp, P_\perp, P_\parallel], \quad (4)$$

which respectively identifies P_\perp and P_\parallel as the pressure components perpendicular and parallel to the magnetic

field. Notice that the anisotropy in T_b^a is produced by the magnetic field B . If this field vanishes, the energy–momentum tensor reduces to that of a perfect fluid with isotropic pressure (an ideal gas of electrons complying with Fermi–Dirac statistics).

The EOS for this magnetized electron gas can be given in the following form [4,11,16]:

$$P_\parallel = -\Omega_e - BM_e + \frac{B^2}{2}, \quad (5)$$

$$P_\perp = -\Omega_e - \frac{B^2}{2}, \quad (6)$$

$$U = -\Omega_e + TS + \mu N + \frac{B^2}{2}. \quad (7)$$

where $M_e = -(\partial\Omega_e/\partial B)$ is the electron-system magnetization, $S = -(\partial\Omega_e/\partial T)$ is the entropy, $N = -(\partial\Omega_e/\partial\mu)$ is the particle number density and the term $B^2/2$ is Maxwell’s classical magnetic contribution. We note that equations (5) and (6) can be re-arranged as [4,9]:

$$P_\perp = P_\parallel - BM, \quad (8)$$

The thermodynamic potential Ω_e can be written as the summ:

$$\Omega_e = \Omega_e^{QFT} + \Omega_e^{SQFT}, \quad (9)$$

where we identify the vacuum term Ω_e^{QFT} , independent of the temperature and chemical potential, and the statistical term, Ω_e^{SQFT} . As is known, Ω_e^{QFT} has non-field-dependent ultraviolet divergencies, hence after renormalizing the Schwinger expression we obtain [17]:

$$\Omega_e^{QFT}(B) = -\frac{1}{8\pi^2} \int_0^\infty \frac{ds}{s^3} \exp(-m_e^2 s) \times \left(esB \coth(esB) - 1 - \frac{(esB)^2}{3} \right), \quad (10)$$

$$\Omega_e^{SQFT}(B, T, \mu) = -\frac{eB}{4\pi^2\beta} \int_{-\infty}^\infty dp_3 \sum_{l=0}^\infty d(l) \ln \left(1 + e^{-\beta(\epsilon_l - \mu)} \right), \quad (11)$$

where $d(l) = 2 - \delta_{l0}$ is the spin degeneracy of Landau levels with $l \neq 0$, m_e is the electron mass, $\epsilon_l = p_3^2 + 2|eB|l + m_e^2$ and $\beta = 1/T$.

Finally, we remark that in a high density regime (which we shall consider henceforth) the contributions to the EOS of the vacuum term and the Maxwell term (*i.e.* Ω_e^{QFT} and $B^2/2$) can be neglected whenever the magnetic field is less than critical (*i.e.* $B < B_c = m_e^2/e$). Thus, in subsequent calculations the leading contribution to the EOS will come from Ω_e^{SQFT} (see Appendix A).

3 Einstein–Maxwell equations

Since we are interested in the critical relativistic regimen, the dynamics of the magnetized gas whose EOS we have

¹ Unless specified otherwise, we use natural units.

described in the previous section must be studied through the Einstein field equations in the framework of General Relativity:

$$G_{\mu\nu} = R_{\mu\nu} - \frac{1}{2}Rg_{\mu\nu} = \kappa T_{\mu\nu}, \quad (12)$$

together with the balance equations of the energy-momentum tensor and Maxwell's equations,

$$T^{\mu\nu}{}_{;\nu} = 0, \quad (13)$$

$$F^{\mu\nu}{}_{;\nu} = 0, \quad F_{[\mu\nu;\alpha]} = 0, \quad (14)$$

where $\kappa = 8\pi G_N$ and G_N is Newton's gravitational constant, while square brackets denote anti-symmetrization in (14).

Assuming absence of annihilation/creation processes, so that particle numbers are conserved, leads to the following conservation equation:

$$n^\alpha{}_{;\alpha} = 0, \quad n^\alpha = N u^\alpha, \quad (15)$$

where N is the particle number density. From the field equations (12) we obtain:

$$-G_x^x = \frac{\dot{Q}_2\dot{Q}_3}{Q_2Q_3} + \frac{\ddot{Q}_2}{Q_2} + \frac{\ddot{Q}_3}{Q_3} = -\kappa P_\perp, \quad (16)$$

$$-G_y^y = \frac{\dot{Q}_1\dot{Q}_3}{Q_1Q_3} + \frac{\ddot{Q}_1}{Q_1} + \frac{\ddot{Q}_3}{Q_3} = -\kappa P_\perp, \quad (17)$$

$$-G_z^z = \frac{\dot{Q}_1\dot{Q}_2}{Q_1Q_2} + \frac{\ddot{Q}_1}{Q_1} + \frac{\ddot{Q}_2}{Q_2} = -\kappa P_\parallel, \quad (18)$$

$$-G_t^t = \frac{\dot{Q}_1\dot{Q}_2}{Q_1Q_2} + \frac{\dot{Q}_1\dot{Q}_3}{Q_1Q_3} + \frac{\dot{Q}_2\dot{Q}_3}{Q_2Q_3} = \kappa U. \quad (19)$$

where $\dot{Q} = Q_{;\alpha}u^\alpha = Q_{,t}$. From the conservation of the energy-momentum tensor (13) we obtain:

$$\dot{U} = - \left(\frac{\dot{Q}_1}{Q_1} + \frac{\dot{Q}_2}{Q_2} \right) (P_\perp + U) - \frac{\dot{Q}_3}{Q_3} (P_\parallel + U). \quad (20)$$

Maxwell's equations (14) yield:

$$\frac{\dot{Q}_1}{Q_1} + \frac{\dot{Q}_2}{Q_2} + \frac{1}{2} \frac{\dot{B}}{B} = 0, \quad (21)$$

and from the particle number conservation (15) leads to:

$$\dot{N} + \left(\frac{\dot{Q}_1}{Q_1} + \frac{\dot{Q}_2}{Q_2} + \frac{\dot{Q}_3}{Q_3} \right) N = 0. \quad (22)$$

4 Local kinematic variables

Einstein-Maxwell field equations are second order system of ordinary differential equations (ODE's). In order to work with a first order system of ODE's, it is useful and convenient to rewrite these equations in terms of covariant kinematic variables that convey the geometric effects on

the kinematics of local fluid elements through the covariant derivatives of u^α . For a Kasner metric in the comoving frame endowed with a normal geodesic 4-velocity, the only non-vanishing kinematic parameters are the expansion scalar, Θ , and the shear tensor $\sigma_{\alpha\beta}$:

$$\Theta = u^\alpha{}_{;\alpha}, \quad \sigma_{\alpha\beta} = u_{(\alpha;\beta)} - \frac{\Theta}{3}h_{\alpha\beta}, \quad (23)$$

where $h_{\alpha\beta} = u_\alpha u_\beta + g_{\alpha\beta}$ is the projection tensor and rounded brackets denote symmetrization. These parameters take the form:

$$\Theta = \frac{\dot{Q}_1}{Q_1} + \frac{\dot{Q}_2}{Q_2} + \frac{\dot{Q}_3}{Q_3}, \quad (24)$$

$$\sigma_\beta^\alpha = \text{diag} [\sigma_x^x, \sigma_y^y, \sigma_z^z, 0] = \text{diag} [\Sigma_1, \Sigma_2, \Sigma_3, 0], \quad (25)$$

where:

$$\Sigma_a = \frac{2}{3} \frac{\dot{Q}_a}{Q_a} - \frac{1}{3} \frac{\dot{Q}_b}{Q_b} - \frac{1}{3} \frac{\dot{Q}_c}{Q_c}, \quad a \neq b \neq c \quad (a, b, c = 1, 2, 3). \quad (26)$$

The geometric interpretation of these parameters is straightforward: Θ represents the isotropic rate of change of the 3-volume of a fluid element, while σ_β^α describes its rate of local deformation along different spatial directions given by its eigenvectors. Since the shear tensor is traceless: $\sigma_\alpha^\alpha = 0$, it is always possible to eliminate any one of the three quantities $(\Sigma_1, \Sigma_2, \Sigma_3)$ in terms of the other two. We choose to eliminate Σ_1 as a function of (Σ_2, Σ_3) .

5 Dynamical equations

By using equations (24) and (26) we can re-write the second derivatives of the metric functions in (16), (17) y (18) as first order derivatives of Θ , Σ_2 and Σ_3 . After some algebraic manipulations it is possible to transform equations (16)-(22) as a first order system of autonomous ODE's:

$$\dot{\Sigma}_2 = \frac{\varkappa}{3} (P_\perp - P_\parallel) - \Theta \Sigma_2, \quad (27)$$

$$\dot{\Sigma}_3 = \frac{2\varkappa}{3} (P_\parallel - P_\perp) - \Theta \Sigma_3, \quad (28)$$

$$\dot{B} = 2B \left(\Sigma_3 - \frac{2}{3}\Theta \right), \quad (29)$$

$$\dot{\mu} = \frac{1}{\text{Det}} [f_1 N_{,T} - f_2 U_{,T}], \quad (30)$$

$$\dot{T} = \frac{1}{\text{Det}} [f_2 U_{,\mu} - f_1 N_{,\mu}], \quad (31)$$

together with the following constraint:

$$\varkappa U = -(\Sigma_2)^2 - \Sigma_2 \Sigma_3 - (\Sigma_3)^2 + \frac{\Theta^2}{3}, \quad (32)$$

where:

$$\text{Det} \equiv U_{,\mu} N_{,T} - U_{,T} N_{,\mu}, \quad (33)$$

$$f_1 = \left(\Sigma_3 - \frac{2\Theta}{3} \right) (P_{\perp} + U) - \left(\Sigma_3 + \frac{\Theta}{3} \right) (P_{\parallel} + U) - U_{,B} \dot{B}, \quad (34)$$

$$f_2 = \Theta N + N_{,B} \dot{B}. \quad (35)$$

We introduce below the following dimensionless evolution parameter,

$$\frac{d}{d\tau} = \frac{1}{H_0} \frac{d}{dt}, \quad \mathcal{H} = \frac{\Theta}{3H_0}, \quad S_2 = \frac{\Sigma_2}{H_0}, \quad S_3 = \frac{\Sigma_3}{H_0}, \quad (36)$$

$$b = \frac{B}{B_c}, \quad \tilde{\mu} = \frac{\mu}{m_e}, \quad \phi = \frac{T}{m_e}, \quad (37)$$

and write the EOS in the form:

$$U = \lambda \Gamma_U (\beta, \tilde{\mu}, \phi), \quad (38)$$

$$P_{\perp} = \lambda \Gamma_{\perp} (\beta, \tilde{\mu}, \phi), \quad (39)$$

$$P_{\parallel} = \lambda \Gamma_{\parallel} (\beta, \tilde{\mu}, \phi), \quad (40)$$

$$N = (\lambda/m_e) \Gamma_{\eta} (\beta, \tilde{\mu}, \phi), \quad (41)$$

where $\lambda = 8\pi m_e / (\lambda_c^3)$ with λ_c the Compton wavelength of the electron and H_0 is a constant with inverse length units that sets the characteristic length scale of the system, which we have chosen as $3H_0^2 = \kappa\lambda \Rightarrow H_0 = 0.86 \times 10^{-10} \text{ m}^{-1}$, so that $1/H_0 \cong 1.15 \times 10^{10} \text{ m}$ is of the order of magnitude of an astronomic unit. It indicates that our simplified model is examined on local scales smaller than cosmic scales. In cosmological sources and models [18] $H_0 = 0.59 \times 10^{-26} \text{ m}^{-1}$ would play the role of the Hubble scale constant, this value is a much greater length scale. The functions S_2 and S_3 are the components of the shear tensor normalized with this scale, while τ is the dimensionless time.

Substituting (36)–(41) into the system (27)–(31) we obtain:

$$S_{2,\tau} = \Gamma_{\perp} - \Gamma_{\parallel} - 3\mathcal{H}S_2, \quad (42)$$

$$S_{3,\tau} = 2(\Gamma_{\parallel} - \Gamma_{\perp}) - 3\mathcal{H}S_3, \quad (43)$$

$$b_{,\tau} = 2b(S_3 - 2\mathcal{H}), \quad (44)$$

$$\tilde{\mu}_{,\tau} = \frac{1}{\text{Det}} \left(\Gamma_{N,\phi} \tilde{f}_1 + \Gamma_{U,\phi} \tilde{f}_2 \right), \quad (45)$$

$$\phi_{,\tau} = -\frac{1}{\text{Det}} \left(\Gamma_{N,\tilde{\mu}} \tilde{f}_1 + \Gamma_{U,\tilde{\mu}} \tilde{f}_2 \right), \quad (46)$$

while the constraint (32) becomes,

$$3\Gamma_U = -S_2^2 - S_3^2 - S_2 S_3 + 3\mathcal{H}^2, \quad (47)$$

and the auxiliary parameters of the previous system take the form:

$$\begin{aligned} \tilde{f}_1 &= (S_3 - 2\mathcal{H})(\Gamma_{\perp} - 2\Gamma_{U,b}) - (S_3 + \mathcal{H})\Gamma_{\parallel} - 3\Gamma_U \mathcal{H}, \\ \tilde{f}_2 &= 3\mathcal{H}\Gamma_N + 2\Gamma_{N,b}(S_3 - 2\mathcal{H}), \\ \text{Det} &= \Gamma_{U,\tilde{\mu}} \Gamma_{N,\phi} - \Gamma_{U,\phi} \Gamma_{N,\tilde{\mu}}. \end{aligned} \quad (48)$$

These differential equations form a complete and self-consistent system whose numeric integration fully determines the variables \mathcal{H} , S_2 , S_3 , b , $\tilde{\mu}$, ϕ , thus allowing us to study the dynamical evolution of a local volume element of a gas of magnetized electrons with finite temperature. In particular, all thermodynamical magnitudes, such as the particle number density, the magnetization, the energy density, the entropy and the pressures, are functions of $b(\tau)$, $\tilde{\mu}(\tau)$, $\phi(\tau)$ and thus can be determined from the numerical solution of this system. On the other hand, \mathcal{H} , S_2 , S_3 provide all the necessary information on the kinematic evolution of volume element, and in particular, its proper volume and the metric functions.

Since $V = \sqrt{-\det g_{\alpha\beta}} = Q_1 Q_2 Q_3$, we obtain by means of (24) and (36) the local volume in terms of \mathcal{H} :

$$V(\tau) = V(0) \exp \left(3 \int_{\tau=0}^{\tau} \mathcal{H} d\tau \right), \quad (49)$$

where we remark that the sign of $\mathcal{H}(\tau)$ implies expansion if $\mathcal{H}(\tau) > 0$, and collapse if $\mathcal{H}(\tau) < 0$. Besides this point, equations (24) and (26) lead to:

$$Q_i(\tau) = Q_i(0) \exp \left[\int_{\tau=0}^{\tau} (\mathcal{H} + S_i) d\tau \right], \quad (i = 1, 2, 3). \quad (50)$$

where $S_1 = -(S_2 + S_3)$. In the following section we undertake the numerical study of the system (42)–(47), focusing specifically on the the collapsing regime.

6 Numeric analysis and physical interpretation

For the numerical study we assume a magnetized electron gas at high density: $\tilde{\mu}_e(0) = 2$, which means that the chemical potential is $2m_e$. The initial values of the magnetic field and temperature were chosen in the ranges $b(0) \sim 10^{-5}$ to $b(0) \sim 10^{-4}$ and $\phi \sim 10^{-6}$ to $\phi \sim 10^{-3}$ respectively². Together with $\mathcal{H}(0) < 0$, we consider the conditions $S_2(0) = 0$, $S_3(0) = 0, +1$, which correspond to the cases with zero initial deformation and initial deformation (shear) in the direction of z axis, respectively. The calculation has been done using the fourth-order Runge–Kutta method with the local truncation relative error less than 10^{-6} .

The numerical solutions for the function \mathcal{H} for the assumed values $\mathcal{H}(0)$ show that $\mathcal{H} \rightarrow -\infty$, which implies that the volume element evolves to a singularity (see equation (49)). This is exemplified in figure 1, where numerical solutions are displayed for the expansion scalar. These curves correspond to different values of the initial temperature in the range $\phi(0) = 10^{-7}$ to $\phi(0) = 10^{-3}$, fixing the rest of the initial conditions on the values $\tilde{\mu}(0) = 2$,

² For instance $B \sim 10^8 \text{ G}$ ($b \sim 10^{-5}$), $T \sim 10^7 \text{ K}$ ($\phi \sim 10^{-3}$) and $\mu \simeq 1 \text{ MeV}$ ($\tilde{\mu} = 2$) correspond to the physical parameters of a white dwarf type astrophysical object.

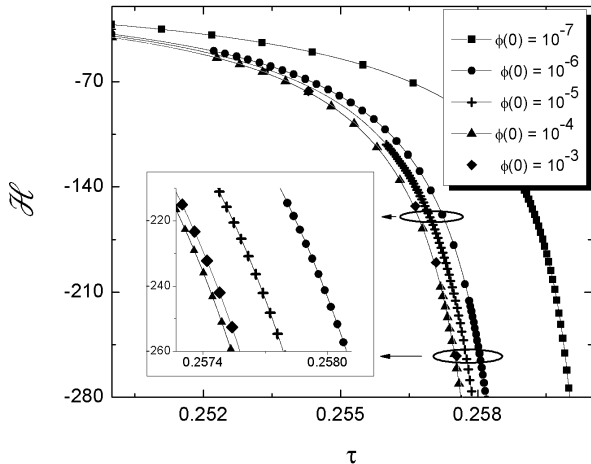


Fig. 1. Numerical solutions for the expansion scalar $\mathcal{H}(\tau)$. The box in the lower corner is an amplification of the graphic.

$b(0) = 5 \times 10^{-5}$, $S_2(0) = 0$ and $S_3(0) = 1$. Notice that in this regime (as given by these initial conditions) where the high densities are dominant, we do not obtain a direct relation between the values of initial temperatures and the collapse time. However, the collapsing time diminishes when the values of the initial magnetic field increases, which agrees with the results obtained in [13], where $T = 0$ was assumed.

In all examined configurations the strength of the magnetic field diverges during the collapse of the volume element, an expected development due to compression of the magnetic fluid. Since the energy-momentum tensor (4) takes the perfect fluid form ($P_{\parallel} = P_{\perp}$) for zero magnetic field, we can identify the magnetic field as the factor introducing anisotropy in the dynamical behavior of the fermionic gas. In particular, this anisotropy in the pressures ($P_{\parallel} \neq P_{\perp}$) must yield different evolution in different directions, which must be evident in a critical stage such as the collapsing regime. When the evolution occurs in such a way that all metric coefficients tend to zero, the singularity is necessarily isotropic “point-like”, whereas when two metric coefficients evolve to zero and the third one to $+\infty$ the result is an anisotropic singularity, “cigar-like” (see the definitions of these types of singularities in [19]). It follows from (50) that the evolution of the terms $S_i + \mathcal{H}$ to $\pm\infty$ implies that the metric coefficient Q_i evolves to either $+\infty$ or 0, which determines the type of singularity. Intuitively, we expect an isotropic point-like singularity if the pressure is isotropic, as pressure diverges in all directions, but a large pressure anisotropy (which necessarily corresponds to large magnetic field) should lead to a qualitatively different direction dependent critical behavior of the pressure, which should result in an anisotropic cigar-like singularity characterized by the divergence of only the pressure parallel to the magnetic field.

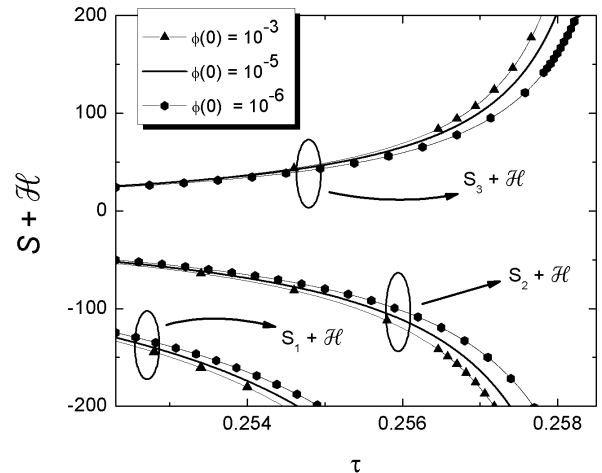


Fig. 2. The plots of the functions $S_i + \mathcal{H}$ for $i = 1, 2, 3$. The system has an initial deformation (shear) in the same direction of the magnetic field: z axis. The collapse is in the form of a “cigar-like” singularity in the z direction.

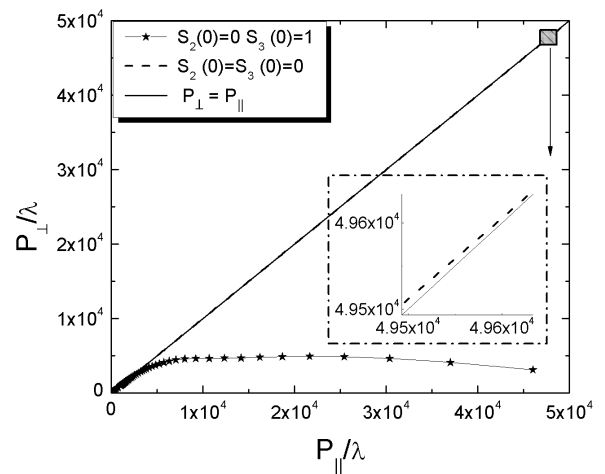


Fig. 3. Pressure parallel and perpendicular to the magnetic field. We plot P_{\parallel}/λ vs P_{\perp}/λ for initial shear $S_2(0) = S_3(0) = 0$ and $S_2(0) = 0 \wedge S_3(0) = 1$ taking $\phi(0) = 10^{-3}$. $\lambda = 8\pi m_e / (\lambda_c^3)$. The case $b = 0$ is shown for reference.

In the numerical calculations whose initial conditions assume zero shear: $S_1(0) = S_2(0) = S_3(0) = 0$, we always obtain a point-like singularity, independently of the selected values for the remaining initial conditions. However, when the initial deformation (shear) is positive in the direction of the magnetic field (z axis), we obtain a cigar-like singularity. Figure 2 displays the solutions of $S + \mathcal{H}$ for initial conditions: $\tilde{\mu}(0) = 2$, $b(0) = 5 \times 10^{-5}$, $S_3(0) = 1$, $S_2(0) = 0$ and $\phi(0) = 10^{-6}, 10^{-6}, 10^{-3}$. The nine curves displayed in the figure correspond to three sets

of functions: $S_i + \mathcal{H}$ ($i = 1, 2, 3$), each one corresponding to three different values of the temperature: $\phi(0) = 10^{-6}, 10^{-5}, 10^{-3}$. As we mentioned previously, in these cases the gas collapses into a cigar-like singularity in the direction of the magnetic field, and when the initial shear is zero the three curves $S_i + \mathcal{H}$ tend to $-\infty$ for each initial value of temperature.

In figure 3 we compare the behavior of the anisotropic pressure in the directions parallel vs perpendicular during the collapse. The dashed line corresponds to the case with zero initial shear, while the star-gray line corresponds to the case of initial positive shear in the z direction. In both cases the remaining initial condition were fixed as: $\phi(0) = 10^{-3}$, $\tilde{\mu}(0) = 2$ and $b(0) = 5 \times 10^{-5}$. As shown by the figure, the pressures exhibit the expected behavior: for initial zero shear we have $P_{\parallel} \approx P_{\perp}$ and a point singularity, but for initial positive shear in the z direction we have a highly anisotropic evolution $P_{\parallel} \gg P_{\perp}$, which signals a cigar-like singularity. The case $P_{\parallel} = P_{\perp}$ with zero magnetic field is shown for comparison (solid line).

For initial values in the range $\phi(0) \sim 10^{-6} - 10^{-4}$ the temperature decreases as the collapse proceeds, while for $\phi(0) \sim 10^{-3}$ and higher values, it increases. This behavior of temperature can be explained by considering that for small initial values ($\phi(0) \sim 10^{-6} - 10^{-4}$) the effects of the magnetic field (alignment of electron spins with the magnetic field) predominate over the effects of temperature (random motion) throughout the whole evolution. Therefore, we argue that the system ‘‘cools down’’ (temperature decreases) during the collapse process as the magnetic field increases. On the other hand, for high initial temperatures ($\phi(0) = 10^{-3}$), the system is ‘‘heated’’ (temperature increases) during the collapse, which shows the predominance of the thermal effect of temperature over the magnetic field effect.

We display in figure 4 two dashed curves for the evolution of the temperature from the initial value $\phi(0) = 10^{-3}$, together with solid curves that depict temperatures starting at $\phi(0) = 10^{-6}$. In both cases the initial conditions correspond to zero initial shear and positive deformation in the z axis. The initial values of magnetic field and chemical potential were fixed at $b(0) = 5 \times 10^{-5}$ and $\tilde{\mu}(0) = 2$ respectively. Notice that the symmetric configuration delays the collapse (yields a longer collapsing time), which may indicate a connection with stability of local fluid elements in compact objects. This could provide an important clue on the stability of a compact object made of a dense magnetized gas. However, verifying this possibility is beyond the scope of this article.

We examine now the behavior of the magnetization and the energy density of the system during the collapse. We remark that the τ -depending functions: b , $\tilde{\mu}$, ϕ follow from the numerical solution of the system (42)–(46) and (47), which allows us to compute the magnetization $M(b, \tilde{\mu}, \phi)$ and $U(b, \tilde{\mu}, \phi)$ for all values of τ . The figures 5 and 6 have been done with the initial conditions: $b(0) = 5 \times 10^{-5}$, $S_2(0) = S_3(0) = 0$.

Figure 5 depicts the behavior of the magnetization vs the magnetic field. Notice how the gas exhibits the de

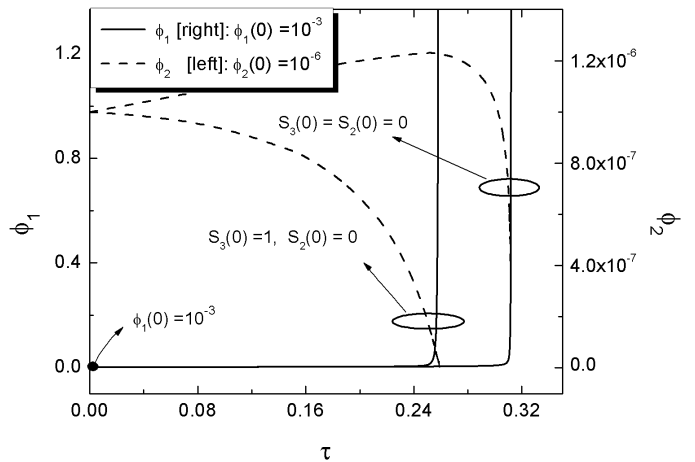


Fig. 4. Temperature of the system. The left hand side of the graph displays the temperature values (ϕ_1) corresponding to the two solid curves. The right hand side displays the temperature values (ϕ_2) corresponding to the two dashed curves.

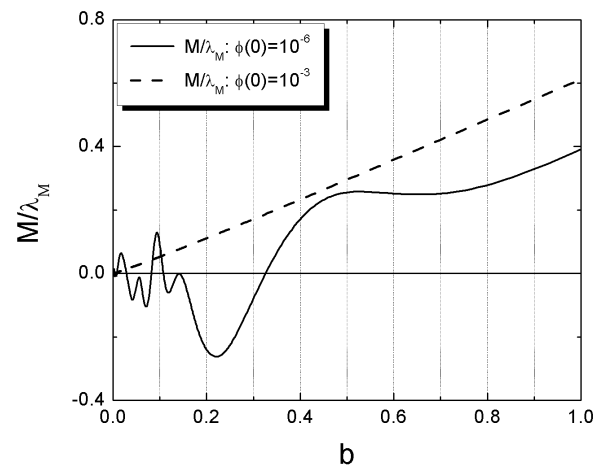


Fig. 5. Magnetization versus magnetic field. The dashed curve (the solid curve) represents the magnetization taking $\phi(0) = 10^{-3}$ ($\phi(0) = 10^{-6}$).

Haas-van Alphen oscillations for small values of the magnetic field and temperature. These oscillations have been observed in many magnetized systems, and are a direct consequence of the Pauli exclusion principle and the discreteness of the spectrum [20]. When the gas starts from initial values $\phi(0) = 10^{-6}$ the magnetization has an oscillatory behavior, with these oscillations disappearing as the magnetic field increases. As a contrast, for initial values $\phi(0) = 10^{-3}$, the system is heated as the collapse proceeds and the magnetization has a non-oscillatory behavior. These results, which were obtained in a time-dependent

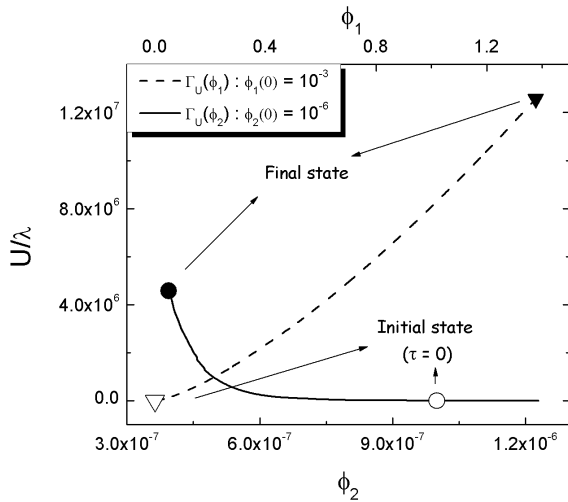


Fig. 6. Energy density versus temperature. The temperature values of the curve drawn with solid line should be observed in the lower axis (ϕ_2) and in the top axis (ϕ_1), those of the curve drawn with dashed line.

system, agree with those obtained in [21, 22], where the authors also studied the magnetization of an electron gas at finite temperature. This agreement shows how the time evolution that we have studied preserves the properties of the same system when it is time-independent.

In all the studied cases the energy density increases as the collapse proceeds, though this fact does not imply that temperature increases. As we have seen above for $\phi(0) = 10^{-3}$, the system is heated during the collapse, which yields a monotonic behavior of the energy density with respect to the temperature. On the other hand, for $\phi(0) = 10^{-6} - 10^{-4}$ the system evolves in such way that temperature decreases in time as energy density increases, without the observed monotonic behavior of the energy density vs the temperature. In this latter case the chemical potential and the particle density increase, even if the temperature decreases and the magnetic field increases. Hence, the energy density also grows during the collapse. Figure 6 displays two curves of the energy density vs temperature, with the dashed and solid line respectively corresponding to $\phi(0) = 10^{-3}$ and $\phi(0) = 10^{-6}$.

It is important to remark that the study we have undertaken here is based on an equation of state and a thermodynamical potential (Ω_e) that come from a one-loop approximation. This approximation may not be appropriate in regimes in which the magnetic field overcomes its critical value. This issue deserves a separate study, possibly in the context of non-perturbative calculations at high magnetic fields, which would mean a different approach that may be applicable to the magnetized gas that we have examined here (see [23] and references quoted therein).

7 Conclusion

We have examined the dynamical and thermodynamical behavior of a magnetized, self-gravitating electron gas at finite temperature, taken as the source of a simplified Bianchi I space-time represented by a Kasner metric, which is the simplest geometry that allows us identify the magnetic field as the main source of anisotropy. We regard this configuration as a toy model that roughly approximates a grand canonical subsystem of a magnetized electron source in the conditions prevailing near of the center and rotation axis of a compact object (in which spatial gradients of physical and kinematic variables may be regarded as negligible). The resulting Einstein-Maxwell field equations were transformed into a system of non-linear autonomous evolution equations, which were solved numerically in the collapsing regime for a chemical potential: $\tilde{\mu} = 2m_e$, a magnetic field in the range $B \sim 10^7 - 10^8$ G and temperatures $T \sim 10^4 - 10^7$ K.

For all initial conditions that we considered the gas evolves into a collapsing singularity, which can be (depending on the initial conditions) isotropic (“point-like”) or anisotropic (“cigar-like”). In all the studied cases the isotropic configuration is the most stable, as the collapsing time is larger. This result may be connected with the stability of volume elements in less idealized configurations, an issue that is outside the scope of this paper and deserves a proper examination elsewhere.

The collapse time decreases as the initial magnetic field increases, but we did not find a direct proportionality relation between this time and the initial temperature (this may be a consequence of having assumed a high density regime).

The behavior of the temperature as the collapse proceeds also depends on initial conditions: for initial temperatures $T \sim 10^4 - 10^6$ K the temperature decreases, while for values $T \gtrsim 10^7$ K the temperature increases. As mentioned previously, this difference in the temperature behavior can be explained by the predominance of the magnetic effects (alignment of electron spins with the magnetic field) over the effects of temperature (random motion) during the evolution of the gas in the regime characterized by low temperature and strong magnetic field.

The behavior of the magnetization and energy density was studied by means of the numerical solutions of the system. We found a monotonic relation between the magnetization and the magnetic field for high temperature values, but this relation does not occur for low temperature values. For small temperature values, when the magnetic field is also small, the electron gas exhibits the Haas-van Alphen oscillations. These results, obtained in a time-dependent system, agree with those obtained in [21, 22] for a time-independent system.

In all the studied cases the energy density increases as the collapse process, even when the system is cooled. This occurs because the particle number density and the chemical potential increase during the collapse, causing the energy density to grow even when the temperature drops.

The study we have presented can be readily applied to examine hadronic systems (complying with suitable balance conditions and adequate chemical potentials). The methodology we have used can also serve as starting point to study the origin and the dynamics of primordial cosmological magnetic fields. These potential extensions of the present work are already under consideration for future articles.

The work of A.P.M, A.U.R and I.D has been supported by *Ministerio de Ciencia, Tecnología y Medio Ambiente* under the grant CB0407 and the ICTP Office of External Activities through NET-35. APM acknowledges to Prof R. Ruffini for his hospitality and financial support at International Center for Relativistic Astrophysics Network-ICRANET. R.A.S. and A.U.R. acknowledge support from the research grant *SEP-CONACYT-132132*, and the TWAS-CONACYT fellowships.

A Contributions to EOS

The thermodynamical potential of an electron gas has two contributions, see equation (9), and thus we can express the magnetization as $M_e = M_{SQFT} + M_{QFT}$. Taking it into account we can rewrite the EOS (42)-(47) in the following form:

$$P_{\parallel} = -\Omega^{SQFT} - BM_{SQFT} - \underbrace{\Omega^{QFT} - BM_{QFT}}_{\frac{B^2}{2}} + \frac{B^2}{2} \\ \equiv \bar{P}_{\parallel}(B, \mu, T) + \Delta P_{\parallel}(B), \quad (51)$$

$$P_{\perp} = -\Omega_{SQFT} - \underbrace{\Omega_{QFT}}_{\frac{B^2}{2}} \\ \equiv \bar{P}_{\perp}(B, \mu, T) + \Delta P_{\perp}(B), \quad (52)$$

$$U = -\Omega_{SQFT} + TS + \mu N - \underbrace{\Omega_{QFT}}_{\frac{B^2}{2}} \\ \equiv \bar{U}(B, \mu, T) + \Delta U(B), \quad (53)$$

where we identify by \bar{P}_{\perp} , \bar{P}_{\parallel} and \bar{U} the terms corresponding to our approximate EOS, while ΔP_{\parallel} , ΔP_{\perp} and ΔU represent those that have been neglected. Note that these last terms are only field-dependent.

In order to analyze the contribution of ΔP_{\parallel} , ΔP_{\perp} and ΔU to its respective EOS, we evaluate the expressions $\bar{P}_{\parallel}/\Delta P_{\parallel}$, $\bar{P}_{\perp}/\Delta P_{\perp}$ and $\bar{U}/\Delta U$ in the sets of solutions obtained previously. In all the cases the numerical results show that these terms are not significant for values of magnetic field less than or equal to the critical magnetic field.

To exemplify that mentioned above, in the figure 7 we show the fractions of the EOS neglected during the evolution of the gas starting from $\phi(0) = 10^{-3}$, $b(0) = 5 \times 10^{-5}$, $\mu(0) = 2$, $S_2(0) = 0$ and $S_3(0) = 1$. As we can observe these values remain near to zero for $B \lesssim B_c$. The graph of magnetic field was included for comparison.

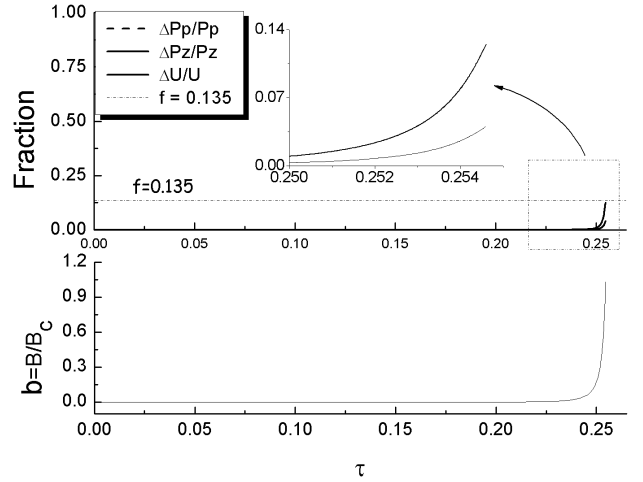


Fig. 7. In the upper (lower) part are shown the fraction of contribution to EOS of the neglected terms (values of magnetic field) versus proper time.

References

1. Stuart L. Shapiro, Saul A. Teukolsky. 1983 "Black Holes, White Dwarfs, and Neutron Stars" ed John Wiley & Sons, Inc.
2. S. Chakrabarty, Phys. Rev. D **43** (1991) 627.
3. S. Chakrabarty, Phys. Rev. D **54** (1996) 1306 [hep-ph/9603406].
4. M. Chaichian, S. S. Masood, C. Montonen, A. Perez Martinez and H. Perez Rojas, Phys. Rev. Lett. **84** (2000) 5261 [hep-ph/9911218].
5. C. Y. Cardall, M. Prakash and J. M. Lattimer, Astrophys. J. **554** (2001) 322 [astro-ph/0011148].
6. R. G. Felipe, H. J. Mosquera Cuesta, A. Perez Martinez and H. Perez Rojas, Chin. J. Astron. Astrophys. **5** (2005) 399 [astro-ph/0207150].
7. A. Perez Martinez, H. Perez Rojas and H. Mosquera Cuesta, Int. J. Mod. Phys. D **17** (2008) 2107 [arXiv:0711.0975 [astro-ph]].
8. L. Paulucci, E. J. Ferrer, V. de la Incera and J. E. Horvath, Phys. Rev. D **83** (2011) 043009 [arXiv:1010.3041 [astro-ph.HE]].
9. A. P. Martínez, H. P. Rojas and H. J. Mosquera Cuesta, Eur. Phys. J. C **29**, 111 (2003).
10. R. G. Felipe and A. P. Martínez, J. Phys. G G **36** (2009) 075202 [arXiv:0812.0337 [astro-ph]].
11. E. J. Ferrer, V. de la Incera, J. P. Keith *et al.*, Phys. Rev. C **82**, 065802 (2010).
12. R. G. Felipe, D. M. Paret and A. P. Martínez, Eur. Phys. J. A **47** (2011) 1 [arXiv:1003.3254 [astro-ph.HE]].
13. A. Ulacia Rey, A. Perez Martinez and R. A. Sussman, Gen. Rel. Grav. **40** (2008) 1499 [arXiv:0708.0593 [gr-qc]].
14. A. Ulacia Rey, A. Perez Martinez and R. A. Sussman, Int. J. Mod. Phys. D **16** (2007) 481 [gr-qc/0605054].
15. D. Manreza Paret, A. Perez Martinez, A. Ulacia Rey and R. A. Sussman, JCAP **1003** (2010) 017 [arXiv:0812.2508 [gr-qc]].

16. H. Y. Chiu, V. Canuto, and L. Fassio-Canuto, Phys. Rev. **176** (1968) 1438; V. Canuto and H. Y. Chiu, Phys. Rev. **173** (1968) 1229; V. Canuto and H. Y. Chiu, Phys. Rev. **173** (1968) 1220; V. Canuto, and H. Y. Chiu, Phys. Rev. **173** (1968) 1210
17. J. Schwinger, Phys. Rev. **82** (1951) 664.
18. Charles. W. Misner, Kip. S. Thorne, John. Archibald. Wheeler, "*Gravitation*," Edit: W. H. Freeman NY, 1998.
19. J. Wainwright, G. F. R. Ellis, "*Dynamical system in cosmology*," ed Cambridge University Press, 1997.
20. D. Ebert, K. G. Klimentko, M. A. Vdovichenko and A. S. Vshivtsev, Phys. Rev. D **61** (2000) 025005 [hep-ph/9905253]; D. Ebert and K. G. Klimentko, Nucl. Phys. A **728** (2003) 203 [hep-ph/0305149].
21. J. O. Andersen, hep-ph/9709331.
22. C. O. Dib and O. Espinosa, Nucl. Phys. B **612** (2001) 492.
23. A. Ayala, A. Sanchez, G. Piccinelli and S. Sahu, Phys. Rev. D **71** (2005) 023004 [hep-ph/0412135].